



Research papers

Tidal creeks as hot-spots for hydrological exchange in a coastal landscape

Clarissa Glaser ^{a,*}, Sven Frei ^b, Gudrun Massmann ^c, Benjamin Silas Gilfedder ^{a,b}^a Limnological Research Station, Bayreuth Center of Ecology and Environmental Research (BAYCEER), University of Bayreuth, Germany^b Department of Hydrology, Bayreuth Center of Ecology and Environmental Research (BAYCEER), University of Bayreuth, Germany^c Institute for Biology and Environmental Sciences, Carl von Ossietzky University of Oldenburg, Germany

ARTICLE INFO

This manuscript was handled by Marco Borga,
Editor-in-Chief

Keywords:
 Submarine groundwater discharge (SGD)
 Radon
 Catchment hydrology
 Subterranean estuary
 Freshwater lens
 Coastal aquifer

ABSTRACT

Coastal ecosystem health and sustainability is tightly coupled to submarine groundwater discharge (SGD) and associated nutrient, carbon and pollutant fluxes. However, there are few studies that systematically analyse the interaction between the terrestrial aquifer system, catchment morphology and coastal SGD. The objective of this study was to evaluate the role of catchment morphology and how this influences the spatial distribution, timing and volume of the SGD flux to a branched tidal creek system, on the barrier island Spiekeroog, Germany. The subsurface salinity was mapped using electrical resistivity tomography (ERT) and a hydrogeochemical survey of the shallow groundwater. Temporal and spatial analysis of geochemical tracers (radon-222, chloride) in the tidal creek water was integrated into a transient ^{222}Rn mass balance model for quantification of SGD rates during two field campaigns that encompassed spring and neap tides. The ERT mapping indicated that fresh groundwater dominated under the dune ridges down to about 15 m depth, but became progressively more brackish seawards. This is likely due to frequent tidal and storm flooding of low-lying areas. The highest groundwater fluxes into the creek were indicated by high ^{222}Rn activities (average 468 Bq m $^{-3}$) towards the dune ridge. Chloride concentrations (up to 17.3 g L $^{-1}$) increased seawards showing the progressive salinization of water in the creek. The freshwater component of SGD was highly variable in time but was highest at low tide, while the total SGD flux (saline + fresh) was highest when tides changed from inflow to outflow as the rapid pressure release on the local aquifer caused a large hydraulic gradient towards the creek. Comparing the freshwater component of mean daily SGD to the creek with estimated groundwater recharge rates in the catchment (665 m 3 d $^{-1}$) shows that the fresh groundwater discharge exceeds fresh recharge during spring tides (~120%) but is lower than recharge during neap tides (~27%). In this study we show that tidal creeks and their relation to catchment morphology are relevant for understanding the spatial and temporal exchange of fresh and saline water between the catchment and coastal zone.

1. Introduction

Exchange of water, and matter (dissolved and particulate) from terrestrial to marine systems is fundamental to hydrological and chemical cycles at the land-sea interface on local to global scales (Burnett et al., 2003, 2006; Cho et al., 2018; Moore, 2010; Sadat-Noori et al., 2016; Webb et al., 2019). Submarine groundwater discharge (SGD) has been identified as an important exchange mechanism between land and sea (Taniguchi et al., 2019). Thus, a mechanistic understanding of the fundamental controls on SGD and associated matter fluxes is required. This has proven challenging because of various complicating factors at the land-sea interface such as variable density flow (Boufadel, 2000), predictable (tides) (Robinson et al., 2007) and unpredictable (storms;

high waves) (Nikpeyman et al., 2019) boundary conditions, and the heterogeneity of material properties in the subsurface (Houben et al., 2018). Especially in tidal and storm affected systems the frequent shifts between saltwater and freshwater interfaces determines the extension of freshwater lenses (Oberdorfer et al., 1990). Dynamic conditions often hamper a sharp delimitation between terrestrial fresh water and seawater that is recycled through the subterranean estuary (Holt et al., 2017). Thus, SGD typically consists of different water components, such as freshwater from inland areas and recirculated sea water (Robinson et al., 2007; Taniguchi et al., 2002). Recirculated sea water often dominates SGD water fluxes (Taniguchi et al., 2019; Robinson et al., 2007), and especially storm tides have been shown to salinize shallow freshwater in the subsurface (Gingerich et al., 2017; Post and Houben,

* Corresponding author at: Center for Applied Geoscience, Eberhard Karls University of Tübingen, Germany.
 E-mail address: clarissa.glaser@uni-tuebingen.de (C. Glaser).

2017). Both salinization and freshwater recharge processes regulate the development and extension of freshwater aquifer systems in the coastal zone (Anderson and Lauer, 2008; Post and Houben, 2017).

Salt marshes are located at the transition zone between terrestrial freshwater and saline water bodies and are usually characterized by vegetation adapted to the gradient in salinity (Wilson et al., 2015a). Tidal creeks cut through low permeable salt marsh mud and directly connect surface waters with underlying aquifers (Krest et al., 2000). In salt marsh areas, recharge by seawater is driven by the inundation of the marsh areas (Wilson and Morris, 2012; Wilson et al., 2015b). This groundwater may then drain into adjoining creeks and rivers (Peterson et al., 2019). Other studies have not observed a direct connection between the flooded surface area and groundwater (e.g. Byers and Chmura, 2014; Harvey et al., 1987). Creeks and tidally influenced rivers may therefore not only drain the groundwater below the salt marsh, but can also connect the coastal hinterland with the sea by acting as a conduit for SGD (Peterson et al., 2010). Consequently, a process based understanding of tidal creeks as an interface between the ocean and terrestrial systems is important for a qualitative and quantitative understanding of nutrient and water cycling between these systems.

System characteristics such as surface topography, spatially non-uniform freshwater recharge and aquifer heterogeneity contribute to the complexity of SGD (Cheng and Ouazar, 2004; Post et al., 2013). Conceptual and physically based models with reduced system complexity can be used to identify primary controls influencing SGD. Both numerical (Greskowiak, 2014; Holt et al., 2019; Houben et al., 2018; Röper et al., 2014b) and physical analogue models (Shi et al., 2011; Stoeckl and Houben, 2012) have provided valuable information on the dominant controls on land-sea interactions. Compared to coastal areas with large and often complex landward catchments, the conditions on islands (including barrier islands) are often much simpler. This is due to the well-defined boundary conditions (surrounded by the ocean) and often a less heterogeneous and complex aquifer system (Anderson and Lauer, 2008). Thus, islands constitute useful conditions for understanding SGD processes and the morphological drivers that influence the exchange of water and solutes in coastal areas.

Various studies have investigated SGD qualitatively and quantitatively using methods such as heat as a tracer (Röper et al., 2014a), isotopes (Cho et al., 2019), geochemical tracers (Hussain et al., 1999; Stieglitz et al., 2010; Taniguchi et al., 2002)), geophysical- (Johnson et al., 2015; O'Connell et al., 2018) and hydraulic methods such as head gradient observations and seepage meters. In this study, our primary objective was to evaluate the role of catchment morphology (dunes, salt marsh and tidal creek system) in influencing the spatial distribution, timing and volume of SGD fluxes. We also aimed to understand the contribution of the tidal creek to the water balance of the coastal aquifer of Spiekeroog. We applied the geochemical tracers radon (^{222}Rn) and chloride (Cl^-) in combination with a spatially lumped, but dynamic ^{222}Rn mass balance model. The barrier island Spiekeroog (Germany) located in the North Sea is a useful experimental field site for SGD studies as the formation and development of the local aquifer system is well studied (e.g. Holt et al., 2017, 2019; Röper et al., 2012).

2. Sampling site

Spiekeroog has a maximum east-west extension of 9.8 km and a maximum width of 2.3 km. The average annual precipitation from 1984 to 2011 for Spiekeroog was 808 mm (OOWV, 2012). The mean tidal range is 2.7 m (Mesotidal) with annual means from 1995 to 2015 of 1.4 m Mean High Water (MHW) asl and 1.3 m bsl Mean Low Water (MLW) (Holt et al., 2017). The freshwater lens below the main dune arc in the western part of Spiekeroog has been subject to prior investigations and is used for the island's public water supply (Röper et al., 2012; Tronicke et al., 1999). In contrast, the freshwater lens in the geologically younger eastern part of the island 'Ostplate' is still under development (Holt et al., 2019; Röper et al., 2013). The Ostplate is characterized by one

main dune arc and a high permeable sandy aquifer combined with nearly no surface run-off in the dunes enhancing groundwater recharge (300–400 mm a⁻¹, Röper et al., 2012). The salt marsh south of the dune arc consists of clay and silt with a low hydraulic permeability (Holt et al., 2019 and references therein). Thus, precipitation in the salt marsh area likely only provides a limited contribution to fresh groundwater recharge (Holt et al., 2017). A relation between vegetation zones and groundwater salinities was recently demonstrated for the Ostplate, where the dominant vegetation serves as a good indicator of the groundwater salinity (Holt et al., 2017). Biogeochemical processes that control the groundwater quality were recently described by Seibert et al. (2019).

The eastern end of the Ostplate is drained by a branched tidal creek (Fig. 1) which extends from the Wadden Sea to the upper salt marsh areas (Holt et al., 2017 and references therein). In total the branched tidal creek network covers an area of around 1 km² (Fig. 1). It consists of one main channel draining in a south-east direction into the Wadden Sea and numerous smaller branches with varying widths and depths. The main stem is about 1 km in length, has a maximum width of 10 m and maximum depth of roughly 0.8 m during low tide. These tidal creeks cut through the mudflat to a depth up to ~1.5 m and expose up to 30 cm of salt marsh mud-clay layer on top of the sandy subsurface sediments.

3. Materials and methods

3.1. ^{222}Rn and electrical conductivity monitoring

Field surveys took place between February 20–26 and March 14–20 2016. ^{222}Rn , electrical conductivity (EC), water level and wind velocity were measured close to the tidal creek mouth (Fig. 1). ^{222}Rn is a sensitive tracer for SGD due to the large contrast in activities between the groundwater and surface water. This contrast is maintained by ^{222}Rn loss by radioactive decay ($t_{1/2} = 3.8$ d) and degassing to the atmosphere from surface water (Taniguchi et al., 2019). ^{222}Rn has been used in numerous studies for quantifying SGD in coastal and estuarine environments (e.g. Burnett et al., 2006; Burnett and Dulaiova, 2003; Sadat-Noori et al., 2018; Stewart et al., 2015; Wong et al., 2013). EC measurements are a simple but useful way to delineate between recycled sea water and fresh water (Short et al., 2015). Sea water measured close to the Spiekeroog harbour, has an EC of ~50 mS cm⁻¹ (Röper et al., 2012), while fresh water under the dunes has a maximum value of 0.1 mS cm⁻¹. For comparability, all EC measurements were converted to equivalent chloride concentrations by correlating measured Cl^- and EC (spatial mapping data) or to salinity based on the method described in Stuyfzand (1993).

^{222}Rn activities were measured continuously using 10 min intervals using a radon-in-air detector (RAD7, Durridge Co.) coupled to a 10 m gas permeable membrane (Accurel® Type PP V8/2 HF, Membrana). The setup is similar to those described in Schubert et al. (2008) and used by Santos et al. (2011). The membrane was wrapped around a PVC tube (20 cm diameter) containing holes (diameter 1 cm) to ensure maximum contact between the membrane and creek water. The membrane was installed in the water column directly above the tidal creek bed and about 2 m away from the bank. A level-logger (Solinst Inc.) was installed next to the membrane which recorded the water level in 5 min intervals. Data from the level logger was atmospherically compensated using a barometric logger (barologger, Solinst Inc.) attached to the RAD7 box. The RAD7 detector was located on a small island in the tidal creek, and was elevated ~50 cm above the ground to reduce the likelihood of flooding during high tide (Fig. 1). The ^{222}Rn distribution between water and air phases at equilibrium depends on water temperature and salinity. The approach introduced by Meyer and Schweidel (1916) with a correction for salinity by Schubert et al. (2012) was used to calculate the ^{222}Rn in water activities from the detected ^{222}Rn in air activities.

Wind velocities were measured 1.25 m above the land surface (5 min intervals) using an anemometer with an integrated data logger at the

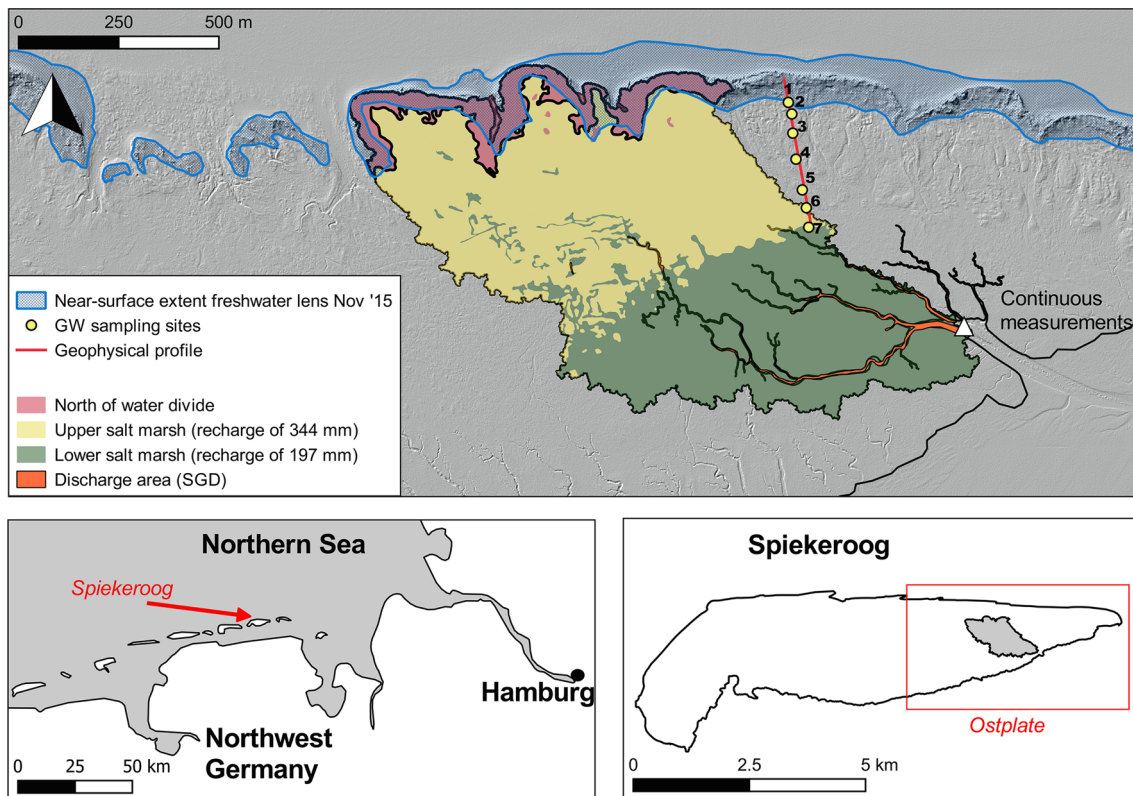


Fig. 1. Investigation area at the island of Spiekeroog with the location of the geoelectrical profile, groundwater (GW) sampling sites, the sampling site of the continuous measurements, and areas in the catchment where recharge and discharge was assumed for comparison of both. The near-surface extent of the freshwater lens (Nov '15) was provided by Holt et al. (2019).

same location. For the second survey in March, wind data was obtained from the 'Deutscher Wetterdienst' due to problems with the data logger. EC was logged at 10 min intervals (Cond 3310, WTW GmbH, Germany) close to the ^{222}Rn measurement site using a floating polystyrene platform.

3.2. ^{222}Rn mass-balance modelling

Quantification of dynamic SGD fluxes were calculated using a ^{222}Rn mass balance approach, similar to the model described in Gilfedder et al. (2015) which was used for wetlands and based on continuous ^{222}Rn measurements. The mass balance model inversely estimates the SGD fluxes by accounting for the wind induced ^{222}Rn losses to the atmosphere as well as the temporal variations in the flooded area of the catchment. The ^{222}Rn mass balance can be written as:

$$\frac{dc_{Rn}}{dt} h \cdot A = (c_{Rn,GW} - c_{Rn}) \cdot Q_{GW} - k_{Rn} \cdot c_{Rn} \cdot A - \lambda \cdot c_{Rn} \cdot h \cdot A + (c_{Rn} - c_{Rn,ocean}) \cdot Q_{flood} - c_{Rn} \cdot Q_{ebb} \quad (1)$$

In Eq. (1), $((c_{Rn,GW} - c_{Rn}) \cdot Q_{GW})$ represents the ^{222}Rn flux from SGD and $((c_{Rn} - c_{Rn,ocean}) \cdot Q_{flood})$ the tidal ^{222}Rn flux into the creek. Degassing of ^{222}Rn into the atmosphere is represented by the term $(k_{Rn} \cdot c_{Rn} \cdot A)$, radioactive decay by the term $(\lambda \cdot c_{Rn} \cdot h \cdot A)$ and tidal outflux under low tide conditions by $(c_{Rn} \cdot Q_{ebb})$. h [m] represents the height of the water column at time step t, A [m^2] the flooded area at time step t, $c_{Rn,GW}$ [Bq m^{-3}] the ^{222}Rn activity of the groundwater (1916 Bq m^{-3} for Spiekeroog according to Santos et al., 2015), Q_{GW} [$\text{m}^3 \text{s}^{-1}$] the SGD flux at time step t and k_{Rn} [m d^{-1}] the gas transfer velocity at time step t, λ [d^{-1}] the first order decay constant for ^{222}Rn (0.181 d^{-1}), $c_{Rn,ocean}$ [Bq m^{-3}] the measured ^{222}Rn activity of the Wadden sea (13 Bq m^{-3}), Q_{flood} [$\text{m}^3 \text{s}^{-1}$] the water flux from the Wadden Sea into the tidal creek at time step t and Q_{ebb} [$\text{m}^3 \text{s}^{-1}$] is the water export from the tidal creek at time step t into

the Wadden Sea during ebb tide. For every time step the flooded area A of the catchment and associated ponded water volume was estimated based on the elevation of the catchment (using LIDAR derived DEM) and the measured water level at sampling site 1. Based on that, Q_{flood} and Q_{ebb} were determined under application of the tidal prism approach (Dyer and Taylor, 1973; Luketina, 1998; Peterson et al., 2010). This approach assumes a uniform water level for the entire catchment area and has been used previously for mangrove systems with similar morphological characteristics (Gleeson et al., 2013).

Determination of the gas transfer velocity (k_{Rn}) for ^{222}Rn was derived from the wind velocity by applying the empirical equation of MacIntyre et al. (1995) (Eqs. (2) and (3)). This is likely to be an underestimate of the real gas exchange fluxes as degassing induced by turbulent flow conditions in the tidal creek is neglected. The original degassing equation proposed by MacIntyre et al. (1995) was developed for degassing of CO_2 . Scaling k from CO_2 to ^{222}Rn was done using the Schmidt number (Sc [-]) ratio and a roughness factor n [-] that accounts for either a smooth or wavy water surface (Eq. (2)). The Schmidt number for any gas is the ratio of the kinematic viscosity to the mass diffusivity. In our case we scaled between k_{600} for CO_2 ($\text{Sc} = 600$ for CO_2 at 20°C) as in MacIntyre et al. (1995) to k_{Rn} by accounting for the effects of water temperature (tidal creek) on the viscosity and diffusivity parameters. A corresponding n value of 0.5 was used representing a wavy water surface at wind speeds $>2 \text{ m s}^{-1}$. The wind velocity U_{10} at 10 m height [m s^{-1}] was calculated assuming a logarithmic wind profile from the measured wind velocity at a height of 1.25 m.

$$k_{Rn} = k_{600} \left(\frac{\text{Sc}_{Rn}}{600} \right)^{-n} \quad (2)$$

$$k_{600} = 0.45 \cdot U_{10}^{1.64} \quad (3)$$

The mass balance in Eq. (1) was solved numerically (Euler method)

and run as a forward model calculating ^{222}Rn activities at each time step of the measurement period. The modelled ^{222}Rn was fitted to the measured data by optimising the SGD flux to the tidal creek at each time step. This is fundamentally different from previous approaches where the mass balance equation is solved explicitly for the SGD fluxes based on measured changes of ^{222}Rn activities in time (i.e. $\Delta^{222}\text{Rn}/\Delta t$) and then adding or subtracting radon source and sink terms (Burnett et al., 2003). We have found that the previous method often results in physically implausible negative groundwater fluxes due to noise in the ^{222}Rn measurements. Previously, these errors have been reduced by e.g. applying smoothing algorithms to the raw data but with an associated loss of temporal resolution (Burnett and Dulaiova, 2003). In some cases negative values have simply been explained by mixing processes between coastal and offshore water with lower ^{222}Rn concentrations which may or may not be the case (Dulaiova et al., 2006).

The optimization method (optimization algorithm *fsolve*; MATLAB) described above has the benefit that 1) it is less sensitive to noise in measurements, 2) it clearly can be seen when the model cannot fit measured data and thus model assumptions are violated, 3) it does not produce negative groundwater fluxes and 4) there is no need to reduce the measurement resolution or applying smoothing algorithms. The disadvantage of this method is the often long simulations times to find the best fit scenario which can range from a few hours to a few days depending on the length of the dataset. A similar approach was applied by Gilfedder et al. (2015) to quantify groundwater discharge to a wetland-lake system and by Dimova and Burnett (2011) for groundwater discharge to a small lake.

A temporal offset of 20 min for measured ^{222}Rn data was used to compensate for the temporal delay to reach equilibrium between ^{222}Rn in the water - and air phase and the formation of the actual measured ^{218}Po on the RAD 7 detector (Stieglitz et al., 2010).

The freshwater component of SGD was calculated based on the Cl^- -concentrations of each sample using a binary mixing model in a similar approach to Salem et al. (2016). The Cl^- ion is assumed to be conservative during the mixing process between freshwater and saline sea water. End member concentrations for the freshwater were assumed to be represented by the samples extracted from under the dunes (0 g L^{-1}) and the sea water end member Cl^- concentrations in the Wadden Sea (16.5 g L^{-1}).

3.3. Spatial mapping in the tidal creek

Water samples from the tidal creek were taken for ^{222}Rn , EC and Cl^- analysis. ^{222}Rn was sampled in 1 L plastic bottles that were filled without headspace from about 5 cm below the water surface. Sample analysis were conducted within a few hours in the island laboratory using a RAD7 (Durridge Company Co.) radon detector (large dome, large detector version) applying the H_2O accessory (Lee and Kim, 2006). The samples were degassed in a closed loop for five minutes and ^{222}Rn decay counts were integrated for one hour. Each sample was counted at least three times with a total measurement time of up to six hours. Results were adjusted for the decay between time of sampling and time of measurement.

The ^{222}Rn and chemical sampling took place in the time frame between 2 h before and after low tide due to regulations limiting access to the National Park during high tide. Distance between sampling locations along the creek were 10–30 m and were selected based on the dominant flow conditions (stagnant water pools and turbulent reaches of the tidal creek system were avoided). EC and temperature was measured directly in the field using a hand-held EC meter (Cond 3310, WTW GmbH, Germany) with an automated temperature correction to 25°C . Cl^- concentration was measured after filtration ($0.45 \mu\text{m}$ filter) in the laboratory of the Limnological Research Station (University of Bayreuth).

3.4. Geoelectrical resistivity surveying and shallow groundwater sampling

An electrical resistivity tomography (ERT) survey (16th of March 2016) and shallow groundwater sampling (18th of March 2016) was performed to determine the spatial extension of the freshwater lens and salinity of the local aquifer below the Ostplate. The ERT transect extended from the dunes to shortly before the start of the tidal creek (Fig. 1). In the NW-SE direction the ERT transect passed through dunes, and upper and lower salt marsh vegetation according to the classification of Holt et al. (2017) (Fig. 1). The ERT estimates the electrical resistivity in the subsurface for 2D profiles which can be used to derive the spatial transition of groundwater salinity (Salem et al., 2016). The total length of the ERT transect was 375 m and consisted of two profiles each using 50 stainless steel electrodes with an electrode spacing of 4 m (4point light 10W, LGM Lippmann). The electrode array configurations included Wenner and dipole-dipole arrays. The subsurface electrical resistivity values were found by inverting the measured apparent resistivity data using Res2dinv software (Geotomo Software 2010) with a least squares inversion algorithm. Shallow groundwater sampling was conducted along the geoelectrical profile at 55 m, 85 m, 132 m, 192 m, 275 m, 321 m and 355 m starting from the northern (dunes) end of the transect (labelled 1–7, respectively, Fig. 7). For sampling, a stainless steel piezometer (diameter of $\sim 2 \text{ cm}$) with a 10 cm screen was hammered $\sim 1.5 \text{ m}$ into the ground. Samples were obtained using a 50 mL syringe and 1.5 m silicone tubing after first purging the piezometer with the syringe and the tubing. The EC was measured directly in the field.

4. Results

4.1. Temporal dynamics of radon, salinity and groundwater discharge to the tidal creek

During spring tide (February 20–26 2016), ^{222}Rn activities ranged from 0 to 315 Bq m^{-3} (Fig. 2(a)). Activities were highest during low tide (Fig. 2 (b)) but rapidly decreased with increasing tidal stage. For the second survey (neap tide), ^{222}Rn activities were not as clearly influenced by the tidal fluctuations, with little variations in ^{222}Rn activities during the four day measurement period (Fig. 3 (a), (b)). ^{222}Rn activities during neap tide were also significantly lower than during spring tide (*t*-test; $p < 0.05$) ranging from 0 to 155 Bq m^{-3} . Simulated and measured ^{222}Rn activities during both surveys showed a very good fit ($R^2 = 0.999$) to measured data. The highest modelled SGD flux up to $84030 \text{ m}^3 \text{ d}^{-1}$ ($\sim 1.2 \text{ m d}^{-1}$) for the first survey (Fig. 2 (d)) and $3125 \text{ m}^3 \text{ d}^{-1}$ ($\sim 0.7 \text{ m d}^{-1}$) for the second survey (Fig. 3 (d)) did not correspond to the highest ^{222}Rn activities at low tide, but were observed when tides change from inflow to outflow conditions (Fig. 2 (d), (e); Fig. 3 (d), (e)). The highest proportion of freshwater in the creek (up to 25%) was observed during low tide and the lowest (up to $\sim 6\%$) for high tide (Figs. 4 and 5).

4.2. Spatial mapping of the tidal creek

Measured ^{222}Rn activities in the tidal creek were highest close to the dunes (mean $468 (\pm 36) \text{ Bq m}^{-3}$), and decreased to below 100 Bq m^{-3} close to the mouth of the creek (Fig. 6). ^{222}Rn activities do not only decrease depending on the distance to the sea (north–south direction), but also decreased away from the main dune arc (east–west direction). The lowest ^{222}Rn activities (17 Bq m^{-3}) were measured for the most western location of the creek. Cl^- concentrations increased during both surveys from the dunes towards the sea, ranging from 9.5 g L^{-1} to 17.3 g L^{-1} for the second survey.

4.3. ERT profile and groundwater sampling

High electrical resistivity values of $160\text{--}400 \Omega\text{m}$ (indicating high freshwater proportions; $< 0.8 \text{ g L}^{-1}$) were measured at the north western

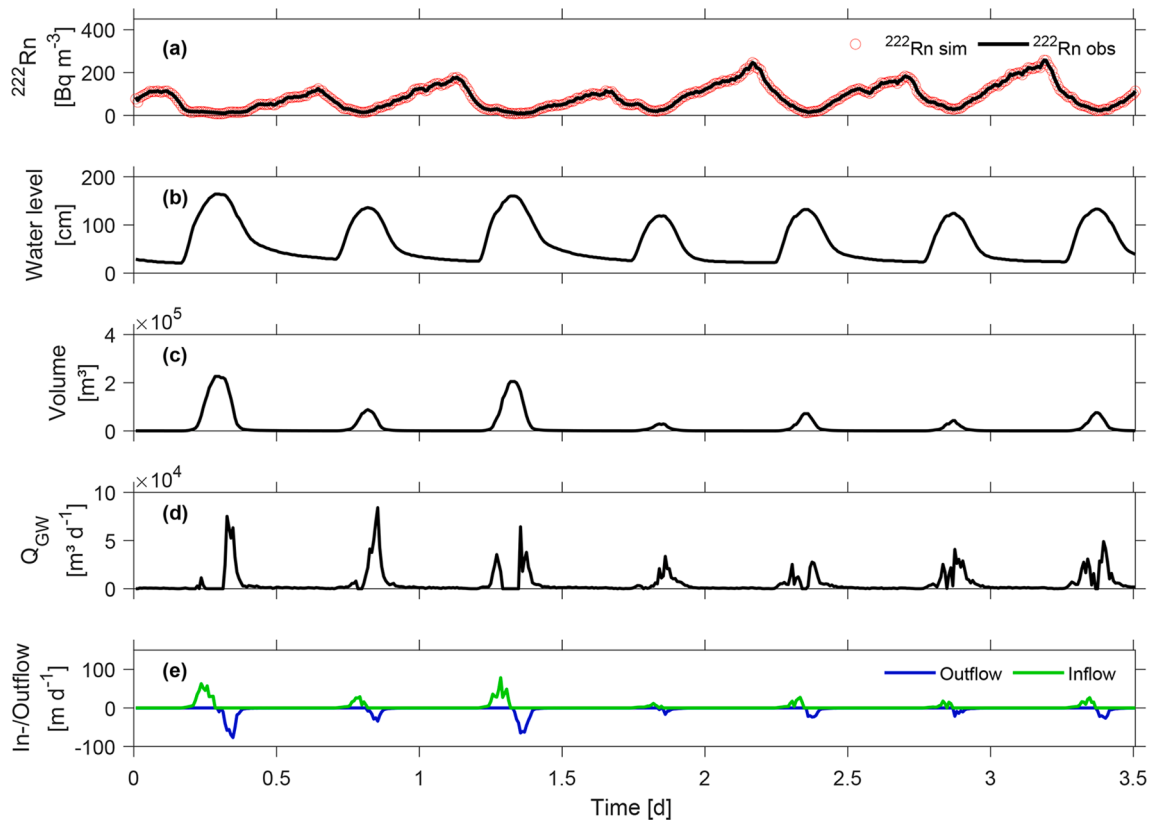


Fig. 2. Simulated and measured ^{222}Rn activities [Bq m^{-3}] (a), water level [cm] (b), surface water volume [m^3] in the catchment (c), modelled submarine groundwater flux Q_{GW} [$\text{m}^3 \text{d}^{-1}$] and flux direction (d), meaning in- or outflow [$\text{m} \text{d}^{-1}$] from or towards the ocean (e) of the first investigation period all with respect to the continuous sampling site.

part of the ERT transect close to the main dune arc (Fig. 1). According to the ERT results, the freshwater lens extended over a total distance of ~ 130 m towards the tidal creek (Fig. 7). ERT results are closely correlated to the salinity measurements for shallow groundwater where low salinities correspond to high electrical resistivity values. Electrical resistivity values along the ERT transect in general decreased towards the sea for the salt marsh, while salinities increased gradually (between 100 and 4 Ωm , salinity 11.2 g L^{-1}).

5. Discussion

5.1. Temporal dynamics of SGD

According to continuous ^{222}Rn and Cl^- data, SGD and fresh SGD fluxes are highly variable in time. ^{222}Rn activities were highest during low tide and rapidly decrease with increasing tidal stage (Figs. 2 and 3). Previous studies have shown that tidal pumping is the primary driving process for SGD during low tide conditions, and is predominantly composed of sea water recycled through the coastal sediments. Tidal pumping is driven by reversal of hydraulic gradients during tidal cycles and describes the infiltration of seawater into intertidal sediments during high tide, and exfiltration during low tide (Gleeson et al., 2013; Li et al., 2009; Robinson et al., 2007; Urich and McKenna, 2004). The high tide sea water reverses the hydraulic gradient towards the aquifer and so restricts groundwater exfiltration and the absence of a SGD flux during high tide. This SGD process seems also plausible for the tidal creek system on the Ostplate (Fig. 8). The highest modelled SGD flux up to 1.2 m d^{-1} for the first and 0.7 m d^{-1} for the second campaign are very high compared to previous studies (e.g. Burnett et al., 2008; Crusius et al., 2005; Nikpeyman et al., 2019). However, average SGD rates of 0.22 m d^{-1} and 0.13 m d^{-1} for the first and second survey, respectively, are comparable to previous investigations quantifying SGD in the western

part of the Island as well as other coastal systems in general (Taniguchi et al., 2002; Burnett et al., 2008; Santos et al., 2015). For example, Santos et al. (2015) estimated a tidally averaged SGD flux of 0.12 m d^{-1} for west Spiekeroog. Calculations suggest the peak fluxes in SGD only occur over a short period of ~ 2 h when tides change from inflow to outflow conditions (Fig. 2 (d); 3 (d)). This can be explained by the large pressure release on the aquifer as water rapidly drains from the creek. This process is amplified by the extreme tidal range (2.72 m for Spiekeroog; Holt et al., 2017), which is distinctive for the Wadden Sea (Marencic, 2009). This peak fluxes in SGD when tides change from inflow to outflow conditions have only seldomly been observed previously, as the volume of the water in the coastal zone (e.g. water in the catchment of the tidal creek) is usually assumed to be constant. In mesotidal creeks in the Wadden sea the assumption of a constant volume is unreasonable due to the large change in the tidal amplitude and associated flooded area ($\Delta A = 0.53 \text{ km}^2$). This is similar to the results of Peterson et al. (2019) where they observed high groundwater inputs during early to mid-ebb tide for a tidal creek with a large tidal amplitude (average 2.4 m). High groundwater inputs were attributed to the increased hydraulic gradient by sea water flooding the marsh. In addition, Peterson et al. (2019) found a relation between the inundation of salt marsh and groundwater input into the creek (no differentiation between fresh or recirculated water). Wilson and Morris (2012) also demonstrated that the volume of groundwater flushing is increased when salt marsh areas get inundated. The groundwater discharge to the tidal creek may be enhanced compared to silty areas in the catchment because creeks cut through the low permeable surface marsh mud (Krest et al., 2000) and thus expose the highly permeable sandy aquifer. On a small scale (< 10 cm), a similar role has been reported for bioturbation due to crab burrows in mangrove systems where preferential groundwater exchange was enhanced by the direct hydrological connection to high permeable sand layers (Gleeson et al., 2013; Stieglitz et al., 2013).

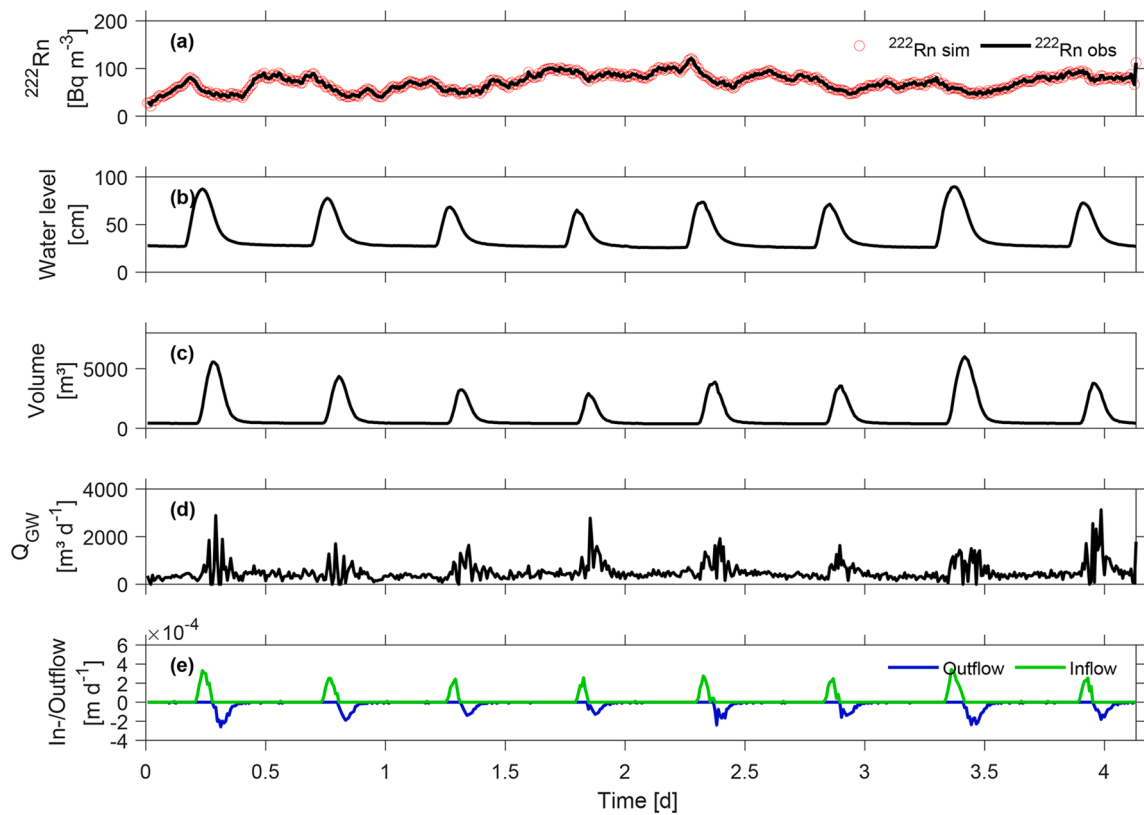


Fig. 3. Simulated and measured ^{222}Rn activities [Bq m^{-3}] (a), water level [cm] (b), surface water volume [m^3] in the catchment (c), modelled submarine groundwater flux Q_{GW} [$\text{m}^3 \text{d}^{-1}$] and flux direction (d), meaning in- or outflow [m d^{-1}] from or towards the ocean (e) of the second investigation period all with respect to the continuous sampling site.

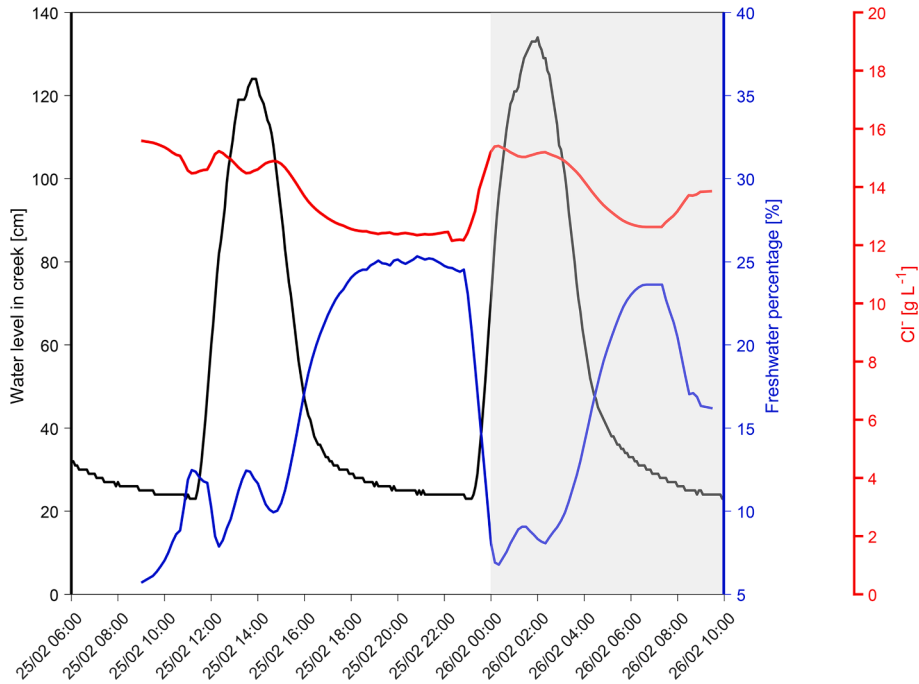


Fig. 4. Tide [cm], Cl^- -concentrations [g L^{-1}] and proportion of freshwater [%] in the creek water during the first investigation period. Due to power failure of the EC measurements (starting from 26/02 10:00) which was used for obtaining Cl^- -concentrations [g L^{-1}], a shorter time-period is presented for the first survey.

The concept is transferable to tidal creeks due to similar settings where the sandy creek bed forms a conductive conduit between the shallow groundwater and the coastal surface water. [Harvey and Odum \(1990\)](#)

suggest that groundwater from sandy aquifers that are topped with salt marsh mud may be directly discharged into creeks through preferential flow paths. Modelling results of [Xin et al. \(2012\)](#) come to a similar

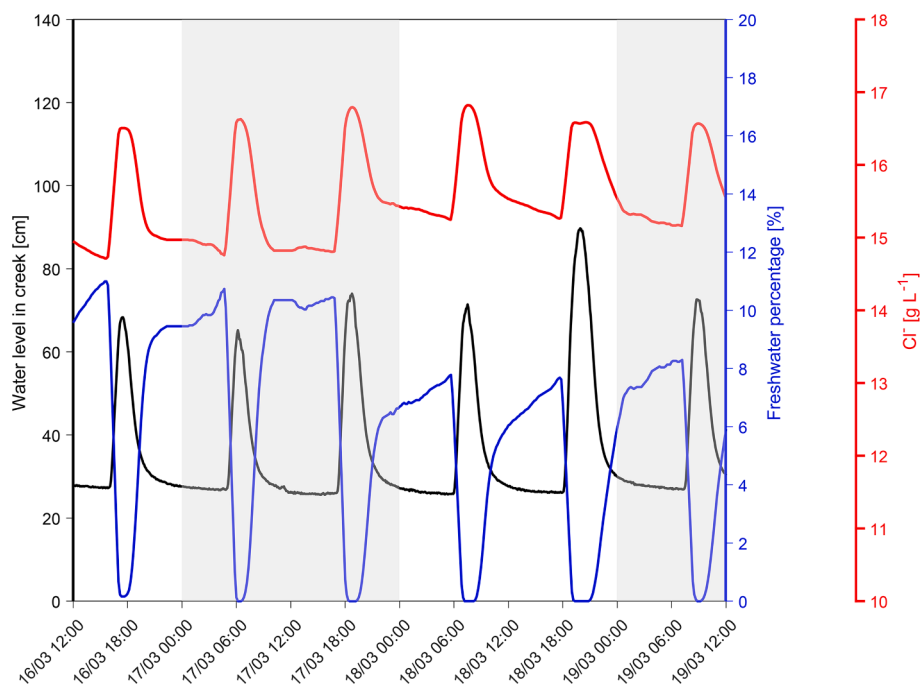


Fig. 5. Tide [cm], Cl^- -concentrations [g L^{-1}] and proportion of freshwater [%] in the creek water during the second investigation period.

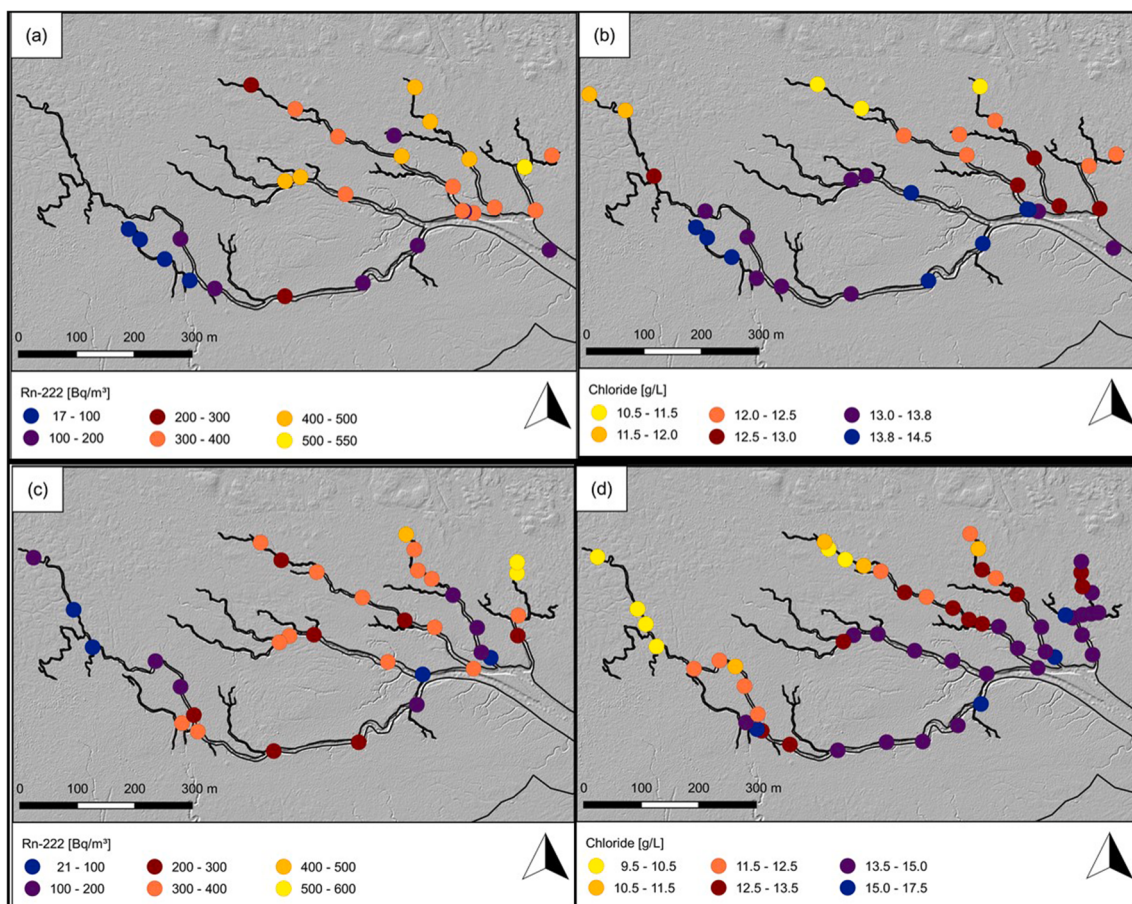


Fig. 6. ^{222}Rn activities [Bq m^{-3}] and Cl^- -concentrations [g L^{-1}] of the investigated tidal creek during the first investigation period (a), (b) (February 20–26 2016) and for the second investigation period (c), (d) (March 14–20 2016).

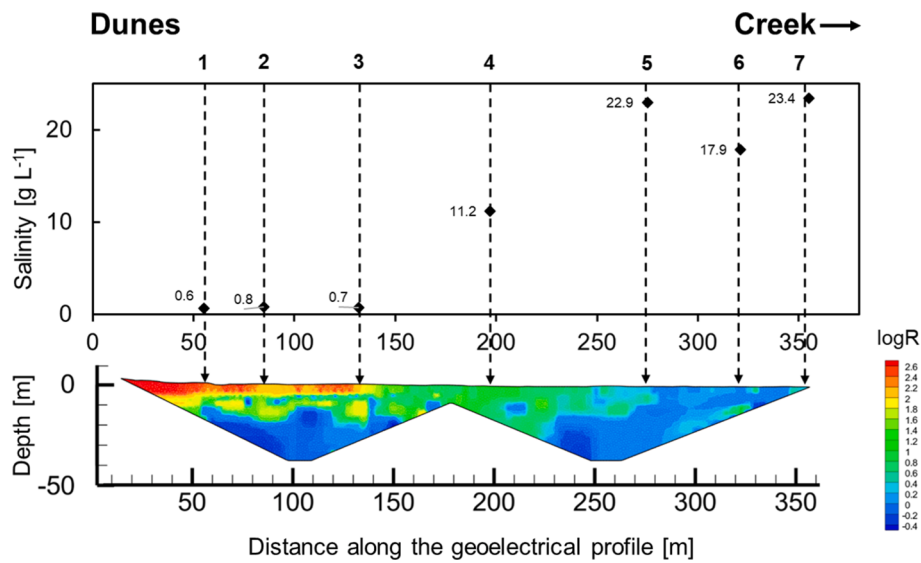


Fig. 7. Geoelectrical profile and Salinity [g L^{-1}] of shallow groundwater along the profile.

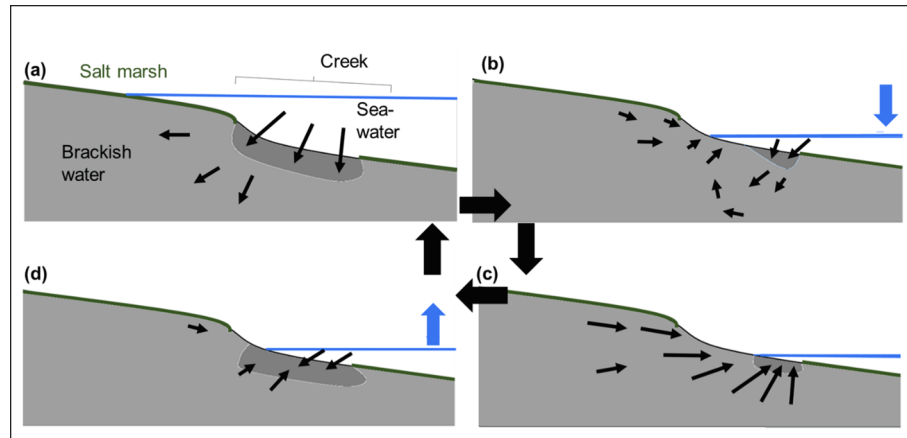


Fig. 8. Conceptual model of the tidal creek. The sandy aquifer with brackish water (bright grey) covered by salt marsh mud (green). During high tide, the hydraulic gradient (black arrows) is towards the aquifer and sea water (dark grey) infiltrates (a). The situation reverses with falling seawater level (b) and water exfiltrates from the aquifer into the sea during low tide situation (c). With raising seawater level (d), the tidal pumping cycle restarts. (For interpretation of the references to colour in this figure legend, the reader is referred to the web version of this article.)

conclusion and show that elastic storage/release mechanisms related to soil compressibility are linked to a change in variations in storage of the aquifer.

The highest proportion of freshwater in the creek (up to 25%) was observed during low tide (Figs. 4 and 5). The small amount of freshwater (~6%) during high tide was attributed to inflowing sea water and water from the last low tide re-entering the creek. This shows that despite the highest proportion of freshwater and the highest ^{222}Rn activities being observed during low tide, the highest SGD fluxes do not necessarily occur at the same time.

5.2. Relation between SGD and groundwater recharge

Spatial measurements of Cl^- and ^{222}Rn allowed the identification of the groundwater origin that contributes to the SGD flux in the creek (Figs. 2 and 3). Low ^{222}Rn activities measured in the tidal creek towards the sea ($<200 \text{ Bq m}^{-3}$) could either be explained by ^{222}Rn decay and degassing during transport, or by dilution with sea water (Fig. 6 (a), (c)). A differentiation between recirculated water and saline sea water from ^{222}Rn data alone is not possible as the accumulation of ^{222}Rn in subsurface waters is independent of water origin and chemistry (Peterson et al., 2019). Higher Cl^- concentrations at seaward sampling sites (Fig. 6 (b), (d)) demonstrate a clear influence of (recirculated) sea water. The fast tidal dynamics (~0.52 days from low to high tide) compared to the

^{222}Rn enrichment in the subsurface (~23 days until equilibrium concentrations are reached) thus suggests that dilution is the dominant factor for low ^{222}Rn activities in the creek close to the sea. However, Cl^- concentration of 13.5 g L^{-1} at the most seaward sampling location during spring tide do not reach the endmember concentration of the Wadden Sea, and the freshwater fraction can still be as high as 18% at this sampling location. This means that either 1) there is a SGD flux beyond the end of the tidal creek directly into the sea or 2) that fresh groundwater entering the creek during low tide remains in the coastal zone close to the end of the creek and flows back into the creek during the next high tide. We favour the second option, as the ^{222}Rn activities in the inflowing tide are also higher than would be expected for the Wadden Sea. Under these conditions small proportion of creek water flows back into the creek system during high tide, similar to what has been described by Crusius et al. (2005).

Close to the dune arc, high ^{222}Rn activities in the tidal creek indicate a higher SGD flux and proportion of groundwater (Burnett et al., 2003; Hussain et al., 1999; Nikpeyman et al., 2019; Swarzenski, 2007). This could be due to a shorter distance to the dunes as the main groundwater recharge area. In addition, the hydraulic gradient arising from the elevation of the dunes is higher (Beukeboom, 1976). According to Holt et al. (2017, 2019) and Röper et al. (2013) there is one major freshwater lens below the dune ridge at the eastern part of the Ostplate, and the eastern branches of the tidal creek are closer to this freshwater lens than

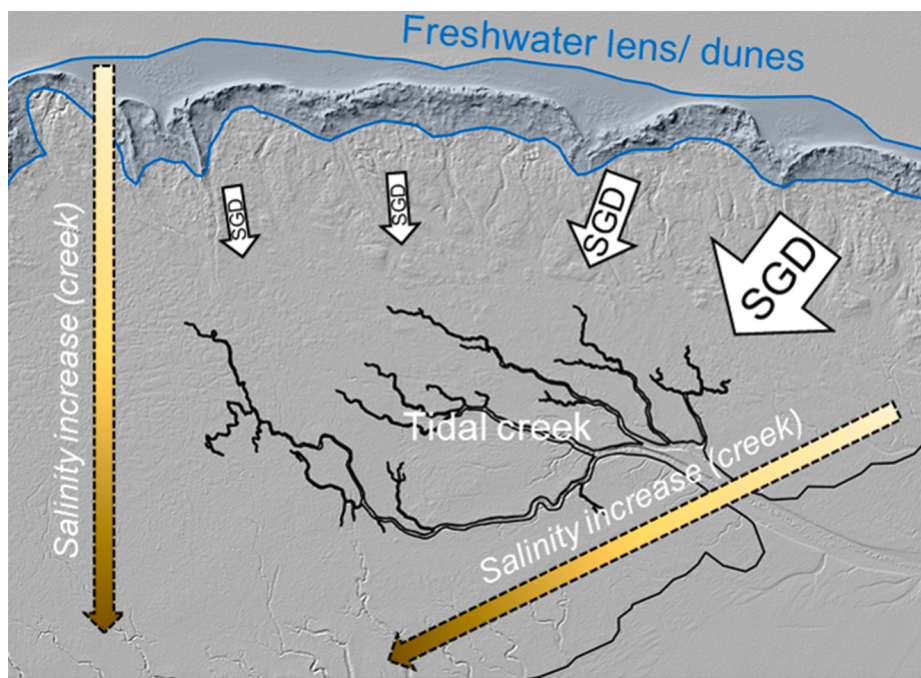


Fig. 9. Conceptual model of the tidal creek catchment representing the preferential fresh groundwater discharge from the dunes into the tidal creek. Groundwater with a high freshwater percentage originates from the dune ridge (white arrows). Brackish proportion of groundwater increases in southern and also western direction (dashed arrow). The extent of the freshwater lens (Nov '2015) is highlighted in blue (Holt et al., 2019). (For interpretation of the references to colour in this figure legend, the reader is referred to the web version of this article.)

the more westerly branches (Fig. 1, Fig. 9). Higher ^{222}Rn activities at the eastern part of the tidal creek (compared to values at the western parts) therefore can be explained by higher fractions of groundwater originating from the nearby freshwater lens below the dune arc to the east (Fig. 9). This indicates that the water in the creek reflects the distance to the underlying freshwater lens under the dune ridges and suggests that discharge into the tidal creek is directly coupled to the main groundwater recharge area and so coupled directly to the dune morphology of the catchment.

5.3. Connection of the creek catchment to the hinterland

The ERT imaging in combination with results from shallow groundwater sampling showed a dominant freshwater component in the aquifer close to the main recharge area under the dunes (Fig. 7). This is in agreement with previous shallow groundwater investigations presented in Holt et al. (2017). ERT imaging results indicate a higher vertical extension of the freshwater lens (10–15 m) than previously reported for the Ostplate (Röper et al., 2013). Recent salinity measurements for shallow groundwater showed a vertical extension of 4–5 m for the freshwater lens (Holt et al., 2017, 2019). However, this study was conducted at the western part of the Ostplate and results may not be transferable to the eastern part (Holt et al., 2017; Röper et al., 2013). The observed gradual increase in the salinity represents an extended transition zone between fresh- and saltwater. The dominance of brackish water rather than a sharp interface between fresh- and saltwater (as seen in other coastal areas) is likely due to (large tides and winter storms) flooding. The high proportion of saltwater in the brackish groundwater can also be attributed to the still developing freshwater lens below the Ostplate (Röper et al., 2013). The origin of the freshwater component in the brackish groundwater below the salt marsh could be rainfall that is preferentially infiltrating (e.g. via bioturbation) (Moffett et al., 2012; Stieglitz et al., 2013; Xin et al., 2012; Xiao et al., 2019). However, this process on the catchment scale is assumed to be of minor relevance for the freshwater fraction in the subterranean estuary (Moffett et al., 2012). Consequently, freshwater recharge for the salt marsh area is low (Wiederhold et al., 2015) due to the low permeability salt marsh clay (Pollmann, 2019). This suggests that most of the freshwater in the brackish groundwater is originated from the local freshwater lens below

the dune arc. As freshwater recharge mainly occurs for the dune area, the morphological setting and terrestrial backdrop of the catchment induced by either the distance to dune recharge area or low topography are pivotal, in addition to the age of the groundwater system in controlling the salinity of the aquifer system.

5.4. Catchment mass-balance and development of the freshwater lens

Differences in simulated groundwater fluxes for the sampling campaigns (Figs. 2 and 3) result from the lower tidal amplitudes during neap tide (second campaign) compared to spring tide conditions (first campaign) (Kim and Hwang, 2002; Li et al., 1999; Urich and McKenna, 2004). Comparison of fresh water recharge rates and fresh water SGD fluxes during neap and spring tides allow an assessment of the tidal creek's role for the catchment's water balance. For estimation of the freshwater recharge, we used the simulation results from a recently developed model of the freshwater lens underneath the Ostplate (Holt et al., 2019). This model suggested that recharge was 344 mm (of which ~69% is freshwater) in the upper saltmarsh, and 197 mm (~41% freshwater) for the lower saltmarsh. Freshwater recharge is assumed to occur evenly distributed over the whole active area (upper salt marsh 0.76 km², lower salt marsh 0.78 km²). Recharge in the dune area (grey dunes) was assumed to drain to the northern beach rather than into the study catchment due to the location of the water divide south of the dunes (Holt et al., 2019). Given these assumptions we calculate a freshwater recharge of 665 m³ d⁻¹ for the creek catchment. Discharge was assumed to only occur into the tidal creek (0.023 km²) due to the direct exposure of the sandy aquifer in the creek bed. Extrapolating the modelled SGD rate of 0.22 m d⁻¹ from the spring tide measurements and a mean SGD freshwater proportion of 16% (Fig. 4) leads to a daily freshwater volume flux of ~810 m³ leaving the aquifer. This shows that ~120% of freshwater recharge drains into the creek during spring tide. For neap tide, a mean SGD rate of 0.13 m d⁻¹ and a freshwater proportion of 6% (Fig. 5) leads to a daily freshwater volume flux of 179 m³ that exits the aquifer via the creek corresponding to only ~27% of fresh water recharge (Table 1). This suggests that a substantial proportion of recharge may contribute to the growth of the freshwater lens at low tidal magnitudes. These simple calculations show that the fresh water balance is highly sensitive to the active recharge area and the temporal

Table 1 Parameters used for comparison of recharge with discharge in the catchment and calculated water proportion [%] and volume [$\text{m}^3 \text{ a}^{-1}$] originated from the freshwater lens exiting via the tidal creek. Recharge and discharge areas were determined according to the dominating biotopes (Biotope map provided by the NLPV). Recharge areas comprise the Upper salt marsh, discharge areas correspond to Pioneer marsh. A water divide was assumed south of the main dune arc based on modelling results of Holt et al. (2019) and not considered for the calculations. An overview of the respective recharge/discharge areas can be found in Fig. 1.

Survey	Recharge			Discharge		
	Mean recharge rate (Holt et al. 2019) [mm a^{-1}]	Mean recharge freshwater proportion (Holt et al. 2019) ¹	Recharge area [km^2]	Aquifer Recharge volume [$\text{m}^3 \text{ d}^{-1}$]	Calculated mean SGD to creek [m d^{-1}]	Fresh water proportion of recharge exiting via the creek [%]
I (Spring tide)	Upper salt marsh	344	~69%	0.76	665	0.023
	Lower salt marsh	197	~41%	0.78		
II (Neap tide)	Upper salt marsh	344	~69%	0.76		
	Lower salt marsh	197	~41%	0.78		

¹Data was obtained from Holt et al. (2019). Freshwater proportion was determined based on the maximum recharge salinity of 32 g L^{-1} , and the mean value of measured salinity distributions from 1975 to 2014 ($6\text{--}16 \text{ g L}^{-1}$, mean 10 g L^{-1} for the upper salt marsh and $16\text{--}22 \text{ g L}^{-1}$, mean 19 g L^{-1} for the lower salt marsh, respectively).

variability in fresh SGD. Even if spring and neap tides are only representative for the maximum and minimum flux values that occur rarely throughout the year, calculations show that there exists a draining capacity of tidal creeks which should not be underestimated, especially for highly vulnerable coastal aquifers.

6. Conclusions

This study demonstrates that tidal creeks are important connectors between areas of groundwater recharge and discharge to the sea. The enhanced hydraulic conductivity of the creek sediment as well as pressure loading effects due to periodic inundation of the salt marsh area is likely to be responsible for the groundwater flux into the tidal creek on the catchment scale. Also the distance to the dunes as groundwater recharge plays a crucial role in that context. Tidal creeks act as a conduit for the freshwater originating from the freshwater lens and in this way increase the freshwater component in the creek system. In contrast, tides and storms lead to salinization of the subterranean estuary below the tidal creek and salt marsh. Comparing fresh groundwater recharge with the fresh SGD into the creek during spring tide and neap tide as regularly occurring maximal and minimal fluxes throughout the year demonstrates that a large proportion of freshwater recharging the lens drains into the Wadden Sea during high tidal magnitudes. During neap tide, a significant amount of freshwater though remains in the aquifer. The comparison of these two extreme tidal situations demonstrates that tidal cycles in creeks have a strong impact on the freshwater extension at barrier islands and thus influence the freshwater occurrence in these sensitive systems.

CRediT authorship contribution statement

Clarissa Glaser: Conceptualization, Investigation, Writing - original draft. **Sven Frei:** Investigation, Writing - review & editing. **Gudrun Massmann:** Writing - review & editing. **Benjamin Silas Gilfedder:** Conceptualization, Investigation, Writing - review & editing.

Declaration of Competing Interest

The authors declare that they have no known competing financial interests or personal relationships that could have appeared to influence the work reported in this paper.

Acknowledgements

This project was supported by the DFG funded KiSNet project, Project number MA7041/6-1. The authors would like to thank the Nationalparkverwaltung Niedersächsisches Wattenmeer (NLPV) for possibility to conduct studies on the Ostplate and the Niedersächsischer Landesbetrieb für Wasserwirtschaft, Küsten- und Naturschutz (NLWKN), mainly Elisabeth Reinke for providing aerial images and laser-scan elevation models. Many thanks to Swantje Fock (Nationalparkhaus Wittbülten at Spiekeroog) for accommodation and to Stefan Durejka for support in sampling. This work was funded using the internal funds of the Limnological Research Station, University of Bayreuth.

References

- Anderson, W.P., Lauer, R.M., 2008. The role of overwash in the evolution of mixing zone morphology within barrier islands. *Hydrogeol. J.* 16 (8), 1483–1495. <https://doi.org/10.1007/s10040-008-0340-z>.
- Beukeboom, Th. J., 1976. The hydrology of the Frisian Islands. (Amsterdam hydrology series), 2nd vol. Brill Rodopi, Amsterdam.
- Boufadel, M.C., 2000. A mechanistic study of nonlinear solute transport in a groundwater-surface water system under steady state and transient hydraulic conditions. *Water Resour. Res.* 36 (9), 2549–2565. <https://doi.org/10.1029/2000WR900159>.
- Burnett, W.C., Aggarwal, P.K., Aureli, A., Bokuniewicz, H., Cable, J.E., Charette, M.A., Kontar, E., Krupa, S., Kulkarni, K.M., Loveless, A., Moore, W.S., Oberdorfer, J.A.,

- Oliveira, J., Ozyurt, N., Povinec, P., Privitera, A.M.G., Rajar, R., Ramessur, R.T., Scholten, J., Stieglitz, T., Taniguchi, M., Turner, J.V., 2006. Quantifying submarine groundwater discharge in the coastal zone via multiple methods. *Sci. Total Environ.* 367 (2-3), 498–543. <https://doi.org/10.1016/j.scitotenv.2006.05.009>.
- Burnett, W.C., Bokuniewicz, H., Huettel, M., Moore, W.S., Taniguchi, M., 2003. Groundwater and pore water inputs to the coastal zone. *Biogeochemistry* 66 (1/2), 3–33. <https://doi.org/10.1023/B:BIOG.0000006066.21240.53>.
- Burnett, W.C., Dulaiova, H., 2003. Estimating the dynamics of groundwater input into the coastal zone via continuous radon-222 measurements. *J. Environ. Radioact.* 69 (1–2), 21–35. [https://doi.org/10.1016/S0265-931X\(03\)00084-5](https://doi.org/10.1016/S0265-931X(03)00084-5).
- Burnett, W.C., Peterson, R., Moore, W.S., Oliveira, J., 2008. Radon and radium isotopes as tracers of submarine groundwater discharge – results from the Ubatuba, Brazil SGD assessment intercomparison. *Estuar. Coast Shelf S* 76 (3), 501–511. <https://doi.org/10.1016/j.ecss.2007.07.027>.
- Byers, S.E., Chmura, G.L., 2014. Observations on shallow subsurface hydrology at bay of fundy macrotidal salt marshes. *J. Coastal Res.* 30 (5), 1006–1016. <https://doi.org/10.2112/JCOASTRES-D-12-00167.1>.
- Cheng, A.H.-D. (Ed.), Ouazar, D. (Ed.), 2004. *Coastal aquifer management - Monitoring, modeling, and case studies*. CRC Press, Boca Raton.
- Cho, H.-M., Kim, G., Kwon, E.Y., Moosdorff, N., Garcia-Orellana, J., Santos, I.R., 2018. Radium tracing nutrient inputs through submarine groundwater discharge in the global ocean. *Sci. Rep.* 8, 2439. <https://doi.org/10.1038/s41598-018-20806-2>.
- Cho, H.-M., Kim, G., Shin, K.-H., 2019. Tracing nitrogen sources fueling coastal green tides off a volcanic island using radon and nitrogen isotopic tracers. *Sci. Total Environ.* 665, 913–919. <https://doi.org/10.1016/j.scitotenv.2019.02.212>.
- Crusius, J., Koopmans, D., Bratton, J.F., Charette, M.A., Kroeger, K., Henderson, P., Ryckman, L., Halloran, K., Colman, J.A., 2005. Submarine groundwater discharge to a small estuary estimated from radon and salinity measurements and a box model. *Biogeosciences* 2, 141–157. <https://doi.org/10.5194/bg-2-141-2005>.
- Dimova, N.T., Burnett, W.C., 2011. Evaluation of groundwater discharge into small lakes based on the temporal distribution of radon-222. *Limnol. Oceanogr.* 56 (2), 486–494. <https://doi.org/10.4319/lo.2011.56.2.0486>.
- Dulaiova, H., Burnett, W.C., Chanton, J.P., Moore, W.S., Bokuniewicz, H.J., Charette, M.A., Sholkovitz, E., 2006. Assessment of groundwater discharges into West Neck Bay, New York, via natural tracers. *Cont. Shelf Res.* 26 (16), 1971–1983. <https://doi.org/10.1016/j.csr.2006.07.011>.
- Dyer, K.R., Taylor, P.A., 1973. A simple, segmented prism model of tidal mixing in well-mixed estuaries. *Estuar. Coast. Mar. Sci.* 1 (4), 411–418. [https://doi.org/10.1016/0302-3524\(73\)90030-3](https://doi.org/10.1016/0302-3524(73)90030-3).
- Gilfedder, B.S., Frei, S., Hofmann, H., Cartwright, I., 2015. Groundwater discharge to wetlands driven by storm and flood events. Quantification using continuous Radon-222 and electrical conductivity measurements and dynamic mass-balance modelling. *Geochim. Cosmochim. Acta* 165, 161–177. <https://doi.org/10.1016/j.gca.2015.05.037>.
- Gingerich, S.B., Voss, C.I., Johnson, A.G., 2017. Seawater-flooding events and impact on freshwater lenses of low-lying islands. Controlling factors, basic management and mitigation. *J. Hydrol.* 551, 676–688. <https://doi.org/10.1016/j.jhydrol.2017.03.001>.
- Gleeson, J., Santos, I.R., Maher, D.T., Golsby-Smith, L., 2013. Groundwater–surface water exchange in a mangrove tidal creek. Evidence from natural geochemical tracers and implications for nutrient budgets. *Mar. Chem.* 156, 27–37. <https://doi.org/10.1016/j.marchem.2013.02.001>.
- Greskowiak, J., 2014. Tide-induced salt-fingerprint flow during submarine groundwater discharge. *Geophys. Res. Lett.* 41 (18), 6413–6419. <https://doi.org/10.1002/2014GL061184>.
- Harvey, J.W., Germann, P.F., Odum, W.E., 1987. Geomorphological control of subsurface hydrology in the creekbank zone of tidal marshes. *Estuar. Coast Shelf S* 25 (6), 677–691. [https://doi.org/10.1016/0272-7714\(87\)90015-1](https://doi.org/10.1016/0272-7714(87)90015-1).
- Harvey, J.W., Odum, W.E., 1990. The influence of tidal marshes on upland groundwater discharge to estuaries. *Biogeochemistry* 10 (3), 217–236. <https://doi.org/10.1007/BF00003145>.
- Holt, T., Greskowiak, J., Seibert, S.L., Massmann, G., 2019. Modeling the evolution of a freshwater lens under highly dynamic conditions on a currently developing Barrier Island. *Geofluids* 2019, 1–15. <https://doi.org/10.1155/2019/9484657>.
- Holt, T., Seibert, S.L., Greskowiak, J., Freund, H., Massmann, G., 2017. Impact of storm tides and inundation frequency on water table salinity and vegetation on a juvenile barrier island. *J. Hydrol.* 554, 666–679. <https://doi.org/10.1016/j.jhydrol.2017.09.014>.
- Houben, G.J., Stoeckl, L., Mariner, K.E., Choudhury, A.S., 2018. The influence of heterogeneity on coastal groundwater flow – physical and numerical modeling of fringing reefs, dykes and structured conductivity fields. *Adv. Water Resour.* 113, 155–166. <https://doi.org/10.1016/j.advwaters.2017.11.024>.
- Hussain, N., Church, T.M., Kim, G., 1999. Use ^{222}Rn and ^{226}Ra to trace groundwater discharge into the Chesapeake Bay. *Mar. Chem.* 65, 127–134. [https://doi.org/10.1016/S0304-4203\(99\)00015-8](https://doi.org/10.1016/S0304-4203(99)00015-8).
- Johnson, C.D., Swarzenski, P.W., Richardson, C.M., Smith, C.G., Kroeger, K.D., Ganguli, P.M., 2015. Ground-truthing electrical resistivity methods in support of submarine groundwater discharge studies. Examples from Hawaii, Washington, and California. *J. Environ. Eng. Geoph.* 20 (1), 81–87. <https://doi.org/10.2113/JEG20.1.81>.
- Kim, G., Hwang, D.-W., 2002. Tidal pumping of groundwater into the coastal ocean revealed from submarine ^{222}Rn and CH_4 monitoring. *Geophys. Res. Lett.* 29 (14), 23–23–4. <https://doi.org/10.1029/2002GL015093>.
- Krest, J.M., Moore, W.S., Gardner, L.R., Morris, J.T., 2000. Marsh nutrient export supplied by groundwater discharge: evidence from radium measurements. *Global Biogeochem. Cy.* 14 (1), 167–176. <https://doi.org/10.1029/1999GB001197>.
- Lee, J.-M., Kim, G., 2006. A simple and rapid method for analyzing radon in coastal and ground waters using a radon-in-air monitor. *J. Environ. Radioact.* 89 (3), 219–228. <https://doi.org/10.1016/j.jenvrad.2006.05.006>.
- Li, L., Barry, D.A., Stagnitti, F., Parlange, J.-Y., 1999. Submarine groundwater discharge and associated chemical input to a coastal sea. *Water Resour. Res.* 35 (11), 3253–3259. <https://doi.org/10.1029/1999WR900189>.
- Li, X., Hu, B.X., Burnett, W.C., Santos, I.R., Chanton, J.P., 2009. Submarine groundwater discharge driven by tidal pumping in a heterogeneous aquifer. *Groundwater* 47 (4), 558–568. <https://doi.org/10.1111/j.1745-6584.2009.00563.x>.
- Luketina, D., 1998. Simple tidal prism models revisited. *Estuar. Coast Shelf S.* 46 (1), 77–84.
- Marencic, H. (Ed.), 2009. Quality Status Report 2009. The Wadden Sea Protection and Management. Common Wadden Sea Secretariat, Trilateral Monitoring and Assessment Group, Wilhelmshaven.
- MacIntyre, S., Wanninkhof, R., Chanton, J.P., 1995. Trace gas exchange across the air-water interface in freshwater and coastal marine environments. In: *Biogenic Trace Gases: Measuring Emissions from Soil and Water* (eds. P. A. Matson and R. C. Hariss). Blackwell Science, 52–57.
- Meyer, S., SchweiDEL, E., 1916. *Radioaktivität*. Springer, Leipzig.
- Moffett, K.B., Gorelick, S.M., McLaren, R.G., Sudicky, E.A., 2012. Salt marsh ecohydrological zonation due to heterogeneous vegetation-groundwater-surface water interactions. *Water Resour. Res.* 48, W02516. <https://doi.org/10.1029/2011WR010874>.
- Moore, W.S., 2010. The effect of submarine groundwater discharge on the ocean. *Annu. Rev. Mar. Sci.* 2 (1), 59–88. <https://doi.org/10.1146/annurev-marine-120308-081019>.
- Nikpeyman, Y., Hosono, T., Ono, M., Yang, H., Ichiyangai, K., Shimada, J., Takikawa, K., 2019. Sea surface waves as a driving force that enhances the fresh shallow coastal groundwater flux into the oceans. *Environ. Earth Sci.* 78 (8), 13. <https://doi.org/10.1007/s12665-019-8258-4>.
- Oberdorfer, J.A., Hogan, P.J., Buddemeier, R.W., 1990. Atoll island hydrogeology. Flow and freshwater occurrence in a tidally dominated system. *J. Hydrol.* 120 (1–4), 327–340. [https://doi.org/10.1016/0022-1694\(90\)90157-S](https://doi.org/10.1016/0022-1694(90)90157-S).
- O'Connell, Y., Daly, E., Henry, T., Brown, C., 2018. Terrestrial and marine electrical resistivity to identify groundwater pathways in coastal karst aquifers. *Near Surf. Geophys.* 16 (2), 164–175. [https://doi.org/10.1002/\(ISSN\)1873-060410.1002/nsg.2018.16.issue-210.3997/1873-0604.2017062](https://doi.org/10.1002/(ISSN)1873-060410.1002/nsg.2018.16.issue-210.3997/1873-0604.2017062).
- OOVV (Oldenburgisch-Ostfriesischer Wasserverband) (2012). Precipitation and Lysimeter Data of Spiekeroog Island from 1984–2011.
- Peterson, R.N., Meile, C., Peterson, L.E., Carter, M., Miklesh, D., 2019. Groundwater discharge dynamics into a salt marsh tidal river. *Estuar. Coast Shelf S* 218, 324–333. <https://doi.org/10.1016/j.ecss.2019.01.007>.
- Peterson, R.N., Santos, I.R., Burnett, W.C., 2010. Evaluating groundwater discharge to tidal rivers based on a Rn-222 time-series approach. *Estuar. Coast Shelf S* 86 (2), 165–178. <https://doi.org/10.1016/j.ecss.2009.10.022>.
- Pollmann, T.D., 2019. Soils and Soil Formation on a temperate Barrier Island (Spiekeroog, southern North Sea coast) Dissertation. Carl von Ossietzky Universität Oldenburg, Germany.
- Post, V.E.A., Groen, J., Kooi, H., Person, M., Ge, S., Edmunds, W.M., 2013. Offshore fresh groundwater reserves as a global phenomenon. *Nature* 504 (7478), 71–78. <https://doi.org/10.1038/nature12858>.
- Post, V.E.A., Houben, G.J., 2017. Density-driven vertical transport of saltwater through the freshwater lens on the island of Baltrum (Germany) following the 1962 storm flood. *J. Hydrol.* 551, 689–702. <https://doi.org/10.1016/j.jhydrol.2017.02.007>.
- Robinson, C., Li, L., Prommer, H., 2007. Tide-induced recirculation across the aquifer-ocean interface. *Water Resour. Res.* 43 (7), 1–14. <https://doi.org/10.1029/2006WR005679>.
- Röper, T., Greskowiak, J., Freund, H., Massmann, G., 2013. Freshwater lens formation below juvenile dunes on a barrier island (Spiekeroog, Northwest Germany). *Estuar. Coast Shelf S* 121–122, 40–50. <https://doi.org/10.1016/j.ecss.2013.02.004>.
- Röper, T., Greskowiak, J., Massmann, G., 2014a. Detecting small groundwater discharge springs using handheld thermal infrared imagery. *Groundwater* 52 (6), 936–942. <https://doi.org/10.1111/gwat.12145>.
- Röper, T., Greskowiak, J., Massmann, G., 2014b. Instabilities of submarine groundwater discharge under tidal forcing. *Limnol. Oceanogr.* 60 (1), 22–28. <https://doi.org/10.1002/ln.10005>.
- Röper, T., Kröger, K.F., Meyer, H., Sültenfuss, J., Greskowiak, J., Massmann, G., 2012. Groundwater ages, recharge conditions and hydrochemical evolution of a barrier island freshwater lens (Spiekeroog, Northern Germany). *J. Hydrol.* 454–455, 173–186.
- Sadat-Noori, M., Santos, I.R., Tait, D.R., Maher, D.T., 2016. Fresh meteoric versus recirculated saline groundwater nutrient inputs into a subtropical estuary. *Sci. Total Environ.* 566–567, 1440–1453. <https://doi.org/10.1016/j.scitotenv.2016.06.008>.
- Sadat-Noori, M., Tait, D.R., Maher, D.T., Holloway, C., Santos, I.R., 2018. Greenhouse gases and submarine groundwater discharge in a Sydney Harbour embayment (Australia). *Estuar. Coast Shelf S.* 207, 499–509. <https://doi.org/10.1016/j.ecss.2017.05.020>.
- Salem, Z.E., Al Temamy, A.M., Salah, M.K., Kassab, M., 2016. Origin and characteristics of brackish groundwater in Abu Madi coastal area, Northern Nile Delta, Egypt. *Estuar. Coast Shelf S.* 178, 21–35. <https://doi.org/10.1016/j.ecss.2016.05.015>.
- Santos, I.R., Beck, M., Brumsack, H.-J., Maher, D.T., Dittmar, T., Waska, H., Schnetterer, B., 2015. Porewater exchange as a driver of carbon dynamics across a terrestrial-marine transect. Insights from coupled ^{222}Rn and $p\text{CO}_2$ observations in the German Wadden Sea. *Mar. Chem.* 171, 10–20. <https://doi.org/10.1016/j.marchem.2015.02.005>.

- Santos, I.R., de Weys, J., Eyre, B.D., 2011. Groundwater or floodwater? assessing the pathways of metal exports from a coastal acid sulfate soil catchment. *Environ. Sci. Technol.* 45 (22), 9641–9648. <https://doi.org/10.1021/es202581h>.
- Schubert, M., Paschke, A., Lieberman, E., Burnett, W.C., 2012. Air-water partitioning of ^{222}Rn and its dependence on water temperature and salinity. *Environ. Sci. Technol.* 46 (7), 3905–3911. <https://doi.org/10.1021/es204680n>.
- Schubert, M., Schmidt, A., Paschke, A., Lopez, A., Balcázar, M., 2008. In situ determination of radon in surface water bodies by means of a hydrophobic membrane tubing. *Radiat. Meas.* 43 (1), 111–120. <https://doi.org/10.1016/j.radmeas.2007.12.017>.
- Seibert, S.L., Greskowiak, J., Prommer, H., Böttcher, M.E., Massmann, G., 2019. Modeling of biogeochemical processes in a barrier island freshwater lens (Spiekeroog, Germany). *J. Hydrol.* 575, 1133–1144. <https://doi.org/10.1016/j.jhydrol.2019.05.094>.
- Shi, L., Cui, L., Park, N., Huyakorn, P.S., 2011. Applicability of a sharp-interface model for estimating steady-state salinity at pumping wells—validation against sand tank experiments. *J. Contam. Hydrol.* 124 (1–4), 35–42. <https://doi.org/10.1016/j.jconhyd.2011.01.005>.
- Short, M.A., Lamontagne, S., Cook, P.G., Cranswick, R., 2015. Characterising the distribution of near-shore submarine groundwater discharge along a coastline using ^{222}Rn and electrical conductivity. *Aust. J. Earth Sci.* 61 (2), 319–331. <https://doi.org/10.1080/08120099.2014.884018>.
- Stewart, B.T., Santos, I.R., Tait, D.R., Macklin, P.A., Maher, D.T., 2015. Submarine groundwater discharge and associated fluxes of alkalinity and dissolved carbon into Moreton Bay (Australia) estimated via radium isotopes. *Mar. Chem.* 174, 1–12. <https://doi.org/10.1016/j.marchem.2015.03.019>.
- Stieglitz, T.C., Cook, P.G., Burnett, W.C., 2010. Inferring coastal processes from regional-scale mapping of ^{222}Rn and salinity: examples from the Great Barrier Reef, Australia. *J. Environ. Radioactiv.* 101 (7), 544–552. <https://doi.org/10.1016/j.jenvrad.2009.11.012>.
- Stieglitz, T.C., Clark, J.F., Hancock, G.J., 2013. The mangrove pump. The tidal flushing of animal burrows in a tropical mangrove forest determined from radionuclide budgets. *Geochim. Cosmochim. Acta* 102, 12–22. <https://doi.org/10.1016/j.gca.2012.10.033>.
- Stoeckl, L., Houben, G., 2012. Flow dynamics and age stratification of freshwater lenses. Experiments and modelling. *J. Hydrol.* 458–459, 9–15. <https://doi.org/10.1016/j.jhydrol.2012.05.070>.
- Stuyfzand, P.J., 1993. Hydrochemistry and hydrology of the coastal dune area of the Western Netherlands. Dissertation, Amsterdam University, Netherlands.
- Swarzenski, P.W., 2007. U/Th series radionuclides as coastal groundwater tracers. *Chem. Rev.* 107 (2), 663–674. <https://doi.org/10.1021/cr0503761>.
- Taniguchi, M., Burnett, W.C., Cable, J.E., Turner, J., 2002. Investigation of submarine groundwater discharge. *Hydrol. Process.* 16 (11), 2115–2129. 10.1002/hyp.1145.
- Taniguchi, M., Dulai, H., Burnett, K.M., Santos, I.R., Sugimoto, R., Stieglitz, T., Kim, G., Moosdorf, N., Burnett, W.C., 2019. Submarine groundwater discharge: updates on its measurement techniques, geophysical drivers, magnitudes, and effects. *Front. Environ. Sci.* 7, 141. <https://doi.org/10.3389/fenvs.2019.00141>.
- Tronicke, J., Blindow, N., Groß, R., Lange, M.A., 1999. Joint application of surface electrical resistivity- and GPR-measurements for groundwater exploration on the island of Spiekeroog—northern Germany. *J. Hydrol.* 223 (1–2), 44–53. [https://doi.org/10.1016/S0022-1694\(99\)00111-0](https://doi.org/10.1016/S0022-1694(99)00111-0).
- Urish, D. W., McKenna, T. E. (2004). Tidal effects on ground water discharge through a sandy marine beach. *Groundwater* 42 (7), 971–982. 10.1111/j.1745-6584.2004.tb02636.x.
- Webb, J.R., Santos, I.R., Maher, D.T., Tait, D.R., Cyronak, T., Sadat-Noori, M., Macklin, P., Jeffrey, L.C., 2019. Groundwater as a source of dissolved organic matter to coastal waters. Insights from radon and CDOM observations in 12 shallow coastal systems. *Limnol. Oceanogr.* 64 (1), 182–196. <https://doi.org/10.1002/lno.11028>.
- Wiederhold, H., Scheer, W., Suzbacher, H., Siemon, B., Kirsch, R., 2015. Nordseeinseln im Klimawandel – die Nordfriesische Insel Föhr und die Ostfriesische Insel Borkum. Aktuelle Küstenforschung an der Nordsee. *Coastline Rep.* 25, 45–48 (in German).
- Wilson, A.M., Morris, J.T., 2012. The influence of tidal forcing on groundwater flow and nutrient exchange in a salt marsh-dominated estuary. *Biogeochemistry* 108 (1–3), 27–38. <https://doi.org/10.1007/s10533-010-9570-y>.
- Wilson, A.M., Evans, T., Moore, W., Schutte, C.A., Joye, S.B., Hughes, A.H., Anderson, J. L., 2015a. Groundwater controls ecological zonation of salt marsh macrophytes. *Ecology* 96 (3), 840–849. <https://doi.org/10.1890/13-2183.110.1890/13-2183.1>.
- Wilson, A.M., Evans, T.B., Moore, W.S., Schutte, C.A., Joye, S.B., 2015b. What time scales are important for monitoring tidally influenced submarine groundwater discharge? insights from a salt marsh. *Water Resour. Res.* 51 (6), 4198–4207. <https://doi.org/10.1002/2014WR015984>.
- Wong, W.W., Grace, M.R., Cartwright, I., Cardenas, M.B., Zamora, P.B., Cook, P.L.M., 2013. Dynamics of groundwater-derived nitrate and nitrous oxide in a tidal estuary from radon mass balance modeling. *Limnol. Oceanogr.* 58 (5), 1689–1706. <https://doi.org/10.4319/lo.2013.58.5.1689>.
- Xiao, K., Li, H., Xia, Y., Yang, J., Wilson, A.M., Michael, H.A., Geng, X., Smith, E., Boufafel, M.C., Yuan, P., Wang, X., 2019. Effects of tidally varying salinity on groundwater flow and solute transport: insights from modelling an idealized creek marsh aquifer. *Water Resour. Res.* 55 (11), 9656–9672. <https://doi.org/10.1029/2018WR024671>.
- Xin, P., Kong, J., Li, L., Barry, D.A., 2012. Effects of soil stratigraphy on pore-water flow in a creek-marsh system. *J. Hydrol.* 475, 175–187. <https://doi.org/10.1016/j.jhydrol.2012.09.047>.